Int. J. Electrochem. Sci., 15 **(2020)** 5362 – 5372, doi: 10.20964/2020.06.63

International Journal of
ELECTROCHEMICAL
SCIENCE
www.electrochemsci.org

2-(2-chlorophenyl)-1H-Benzimidazole as a New Corrosion Inhibitor for Copper in Sulfuric Acid

Jinliang Zhang[1,*], *Hao Li*[2]

[1] School of Materials and Chemical Engineering, Ningbo University of Technology, Ningbo Zhejiang 315211, China
[2] School of Chemistry and Chemical Engineering, Chongqing University, Chongqing, 400044, China
[*]E-mail: zhangjinliang_nut@126.com

Received: 11 January 2020 / *Accepted:* 10 March 2020 / *Published:* 10 May 2020

A benzimidazole derivative namely 2-(2-chlorophenyl)-1H-Benzimidazole (CPBI) was investigated for corrosion inhibition of copper in 0.5 mol L^{-1} H_2SO_4 solution using electrochemical methods, scanning electron microscope (SEM), and laser scanning confocal microscope (LSCM). We found that the adsorption of CPBI molecules on copper conforms to a Langmuir type adsorption isotherm and belongs to a mixed type inhibitor. With the addition of 5 mmol L^{-1} CPBI, the maximum efficiencies of 92.3% was obtained, whereas 5 mmol L^{-1} benzimidazole (BIM) only have 70.1% ability. The topography maps of SEM and LSCM are consistent with the electrochemical results. In addition, molecular dynamics simulation and quantum chemical calculation further reveal the adsorption and inhibition mechanism of CPBI from a microscopic level.

Keywords: Corrosion inhibition, Copper, acid, Langmuir isotherm, MD

1. INTRODUCTION

Copper has favorable thermal, conductive conductivity, and its malleability and ductility are also better [1-3]. Thus, it is usually used to produce manufacturing industrial valves, pumps, heat exchangers, molds, sliding bearings, and so on. However, copper materials can easily be oxidized and corroded in humid air, resulting in many scale and rust on copper surface. As an efficient method for cleaning metal surfaces, acid pickling has been widely used for removing the oxides, rust and dirt [4-6]. In this case, sulfuric acid is often used [7, 8].

However, dilute sulfuric acid dissolving oxygen can corrode the copper substrate and then damage the copper equipment. Among many techniques to prevent corrosion of metals, using inhibitors

has become the most important method to slow down the corrosion of metal in pickling process because of the simple, economical and convenient properties [9-13].

In past decades, various pickling corrosion inhibitors for copper have also been continuously developed and utilized [14, 15]. Most organic compounds contain unsaturated bonds and atoms, such as N, S, O and so on, have been investigated as effective corrosion inhibitors [16-19]. These heteroatoms will accelerate inhibitor molecules to adsorb on metal surface, thus expelling the corrosion medium from attacking the metal substrate. Qiang et al. proposed four ionic liquids and carbon quantum dots as high-efficiency copper corrosion inhibitors in sulfuric acid solution by various experimental and computational methods [1, 20]. He gives the new insights into the inhibition mechanism at atomic level and significantly advances the field of organic pickling corrosion inhibitors. Tan et al. also studied the inhibition effect of a drug Montelukast on the copper corrosion in H_2SO_4 solution [21].

In this work, the anticorrosive behavior of a benzimidazole derivative namely 2-(2-chlorophenyl)-1H-Benzimidazole (CPBI) was evaluated. The inhibition effect for copper in 0.5 M sulfuric medium was studied by using electrochemical impedance measurements (EIS), polarization curves, scanning electron microscope (SEM), and laser scanning confocal microscope (LSCM). In addition, quantum chemical calculation and molecular simulation were applied to elicit the inhibition mechanism of the CPBI.

2. EXPERIMENTAL

2.1 Material and electrochemical measurements

For electrochemical tests, copper electrode with the purity of more than 99.5% was measured. The copper was sealed with epoxy resin, and the working surface was 1 × 1 cm. The copper surface was polished with SiC sandpaper until 2000 mesh. It was degreased with acetone, swashed with deionized water, dried at room temperature in an air stream, and finally placed in a desiccator. CHI760e electrochemical workstation with a three-electrode system was used, consisting of the reference electrode (saturated calomel electrode), working electrode (copper), and the platinum counter electrode. The 0.5 mol L^{-1} H_2SO_4 was prepared using ultrapure water and concentrated H_2SO_4. CPBI shown in Fig. 1 was dissolved in 0.5 mol L^{-1} H_2SO_4 (0.5, 1, 2, and 5 mmol L^{-1}). After open circuit potential (OCP) test, AC impedance was evaluated from 0.01 Hz to 100000 Hz on stable OCP value and the excitation signal is 5 mV sine wave. The polarization curves were measured with a polarization range of ± 250 mV VS.OCP at a scan rate of 1 mV.

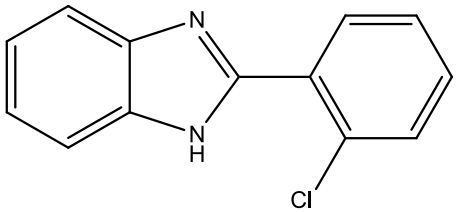

Figure 1. The chemical structure of CPBI.

2.2 Surface tests

SEM (JEOL-JSM-7800F) and LSCM was applied to observe the surface morphology of copper specimens in the absence and presence of CPBI. Before testing the SEM, the copper cubes were sanded sequentially to 7000 mesh on sand paper to obtain smooth surface. And then soaked in a constant temperature water bath at 298 K for 48 hours in 0.5 mol L^{-1} sulfuric acid containing and not containing 5 mmol L^{-1} CPBI. Similarly, for LSCM, the copper sheets were treated in the same way as the SEM and the specimen immersion time is 12 hours.

2.3 Calculation parameters

CPBI molecule structure was optimized by DMol3 module from Material Studio basing density functional theory (DFT). The molecular frontier orbital and related parameters were obtained including the energy of highest occupied molecular orbital (E_{HOMO}), the energy of lowest unoccupied molecular orbital (E_{LUMO}), the dipole moment (μ), and energy gap ($\Delta E = E_{LUMO} - E_{HOMO}$). The process of adsorbing CPBI molecule on copper surface is simulated with Forcite module to explore the interaction between CPBI and Cu (111) surface. The calculation parameters were NVT ensemble, 1 fs time step size and 400 ps simulation time at 298 K. The maximum number of convergences is 500, COMPSS force field and Electrostatic and Van der Waals are choosing.

3. RESULTS AND DISCUSSION

3.1 Potentiodynamic polarization curves

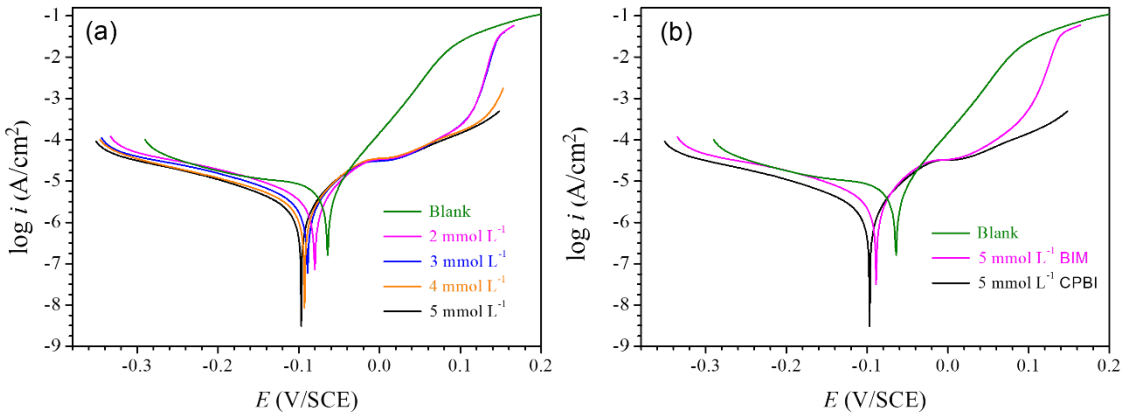

Figure 2. Potentiodynamic polarization curves of copper in 0.5 mol L^{-1} sulfuric acid (a) with CPBI and the (b) compared with BIM at 298 K.

Potentiodynamic polarization plots of copper in 0.5 mol L^{-1} sulfuric acid with and without CPBI at 298 K are shown in Fig. 2a. With the addition of CPBI and increasing concentration from 0.5 mmol L^{-1} to 5 mmol L^{-1}, it can be seen that the corrosion current density decreases significantly and the corrosion potential shifts to negative direction, which indicates that CPBI have a stronger influence on

reducing the oxygen cathode than copper oxidation reaction [22]. In addition, Fig. 2b shows the comparison of CPBI and BIM, indicating the better inhibitive ability of CPBI than BIM.

The Tafel parameters including i_{corr} (corrosion current density), η (inhibition efficiency) E_{corr} (corrosion potential), β_a (anodic Tafel slope) and β_c (cathodic Tafel slope) were summarized and listed in Table 1. The inhibition efficiency can be obtained by:

$$\eta(\%) = (1 - \frac{i_{corr}}{i_{corr,0}}) \times 100 \quad (1)$$

where $i_{corr,0}$ and i_{corr} is current densities of bare copper and with inhibitor adsorption, respectively.

From Table 1, we can clearly see that i_{corr} values decrease with the CPBI addition. The values of i_{corr} continue to decease and the η values add with incremental concentration of studied CPBI. At 5 mmol L^{-1} CPBI concentration, i_{corr} value reached the minimum value of 2.34 μA cm^{-2}, and inhibition efficiency can reach the maximum value of 83.1%. Besides, all corrosion potential at 298 K with different concentrations of CPBI moves less than 30 mV (＜85mV), showing that CPBI belongs to a mixed-type inhibitor [23]. As a comparison, the traditional corrosion inhibitor BIM only provided best 62.1% protective ability at 5 mmol L^{-1}. Therefore, it can be inferred that a dense and orderly CPBI protective film was formed on Cu, effectively preventing corrosion from acid medium.

Table 1. Tafel parameters of copper in 0.5 mol L^{-1} sulfuric acid with CPBI and BIM.

Inhibitor	C(mmol L^{-1})	E_{corr}(V/SCE)	i_{corr}(μA cm^{-2})	β_c(mV dec^{-1})	β_a(mV dec^{-1})	η(%)
	Blank	–0.064	13.9	–428	41	–
	0.5	–0.080	4.17	–134	67	70.0
CPBI	1	–0.089	3.49	–131	66	74.9
	2	–0.093	2.76	–118	62	80.1
	5	–0.097	2.34	–112	61	83.1
BIM	5	–0.089	4.51	–142	70	62.1

3.2 EIS

Nyquist plots for copper in 0.5 M sulfuric acid in the absence and presence of various concentrations of CPBI are presented in Fig. 2. For blank curve, the spectrum consists a semicircle of capacitive type followed with a Warburg impedance. After the addition of CPBI, the Warburg impedance is disappeared and the impedance response was represented by only capacitive type. Besides, the radius of the capacitive arc increases significantly with increasing CPBI concentration. This is because the CPBI adsorption on the surface of copper electrode resulted in the formation of a dense and ordered protective film, so that the dissolution of the anode copper became difficult and the corrosion resistance of the electrode increased [24]. It is noted that the shape of the impedance plot with inhibitor is similar, indicating that the corrosion mechanism of copper was not changed by CPBI addition [25, 26]. Fig. 2b also shows the bigger impedance radius of CPBI than BIM at 5 mmol L^{-1}, which indicates the better protection performance of studied CPBI inhibitor.

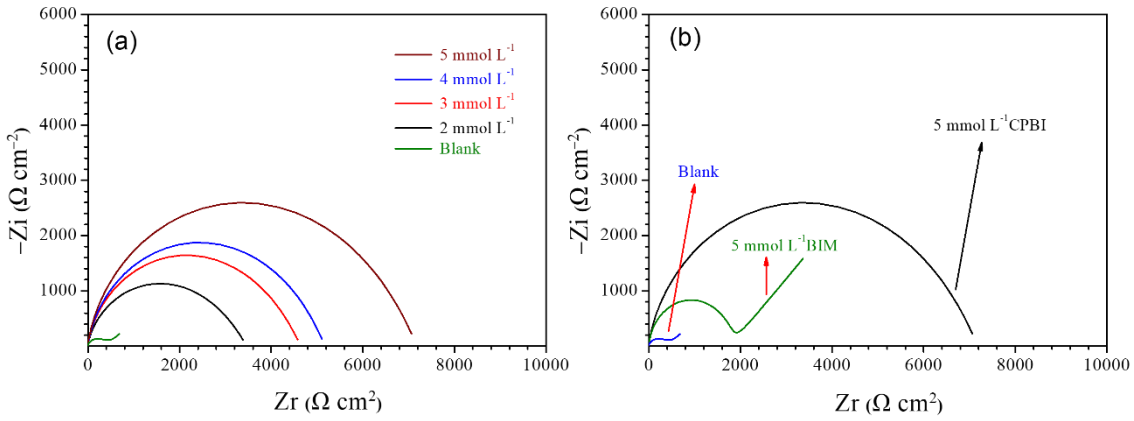

Figure 3. Nyquist diagrams of copper in 0.5 mol L^{-1} sulfuric acid (a) with CPBI, (b) compared with BIM

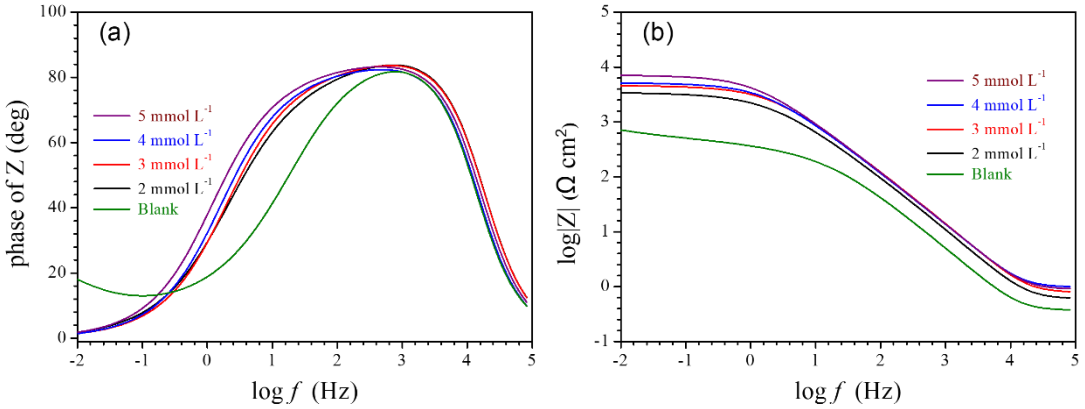

Figure 4. Bode plots of copper in 0.5 mol L^{-1} sulfuric acid with CPBI: (a) phase angle, (b) modulus.

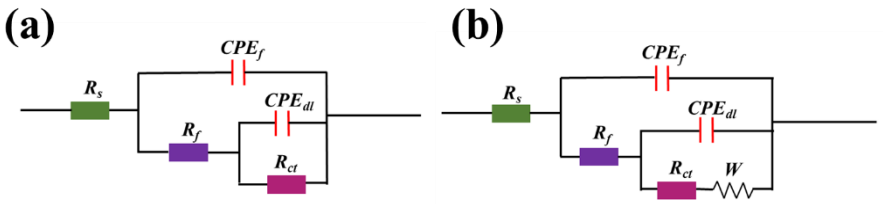

Figure 5. Equivalent circuit diagrams for AC impedance.

Bode plots in the absence and presence of CPBI are presented in Fig. 4. With increasing concentration of CPBI, the impedance modulus bigger and the phase angle become remarkably larger. The AC impedance parameters are simulated according to the equivalent circuit (Fig. 5), which includes charge transfer resistance (R_{ct}), film resistance (R_f) and a constant phase element (*CPE*). The double layer and film capacitance (C_{dl} and C_f) value simulated from *CPE* value. The capacitance *C* was calculated by [1]:

$$C = Y_0 (\omega)^{n-1} = Y_0 (2\pi f_{\text{Zim-Max}})^{n-1} \quad (2)$$

The inhibition efficiencies are determined as following equation,

$$\eta(\%) = (1 - \frac{R_{p,0}}{Rp}) \times 100 \quad (3)$$

where R_p and $R_{p,0}$ are the sum of R_f and R_{ct} with and without CPBI.

Table 2. EIS parameters for copper in 0.5 mol L^{-1} sulfuric acid at 298 K with different CPBI concentration compared with BIM.

	C (mM)	R_f (Ω cm^2)	R_{ct} (kΩ cm^2)	R_p (kΩ cm^2)	C_f (μF cm^{-2})	n_1	C_{dl} (μF cm^{-2})	n_2	W	η (%)
	Blank	0.4	0.56	0.56	50.1	0.4	62.3	1	1.29	—
	0.5	106	3.36	3.47	14.3	1	60.8	0.59	—	83.8
CPBI	1	112	4.54	4.65	11.1	1	34.7	0.62	—	87.9
	2	171	5.11	5.28	11.1	1	31.6	0.65	—	89.4
	5	168	7.12	7.29	11.0	1	28.1	0.5	—	92.3
BIM	5	81	1.79	1.87	14.2	0.95	51.0	0.55	6.47	70.1

All fitted parameters are listed in Table 2. Obviously, the values of C_f and C_{d1} decreased dramatically with the concentrations of CPBI increases, because that water molecules on the copper surface were replaced by CPBI molecules. After addition and increased concentration of CPBI, the formation of a protective CPBI film on the electrode surface reduces the exposed copper area in the corrosive medium and increasing the thickness of the CPBI film, resulting in the decrease of C_f and C_{dl} values [16, 27, 28]. Moreover, it can be seen that the values of R_{ct} and R_f are much bigger for inhibited conditions as compared to those values of uninhibited condition, manifesting the formation of inhibitor-adsorption film of CPBI on copper substrate. For CPBI, the η value reaches 92.3% at 5 mmol L^{-1} from 83.8% at 0.5 mmol L^{-1}, whereas BIM has lower inhibitive ability of 70.1% at 0.5 mmol L^{-1}. This is consistent with the Potentiodynamic polarization curve results above.

3.3 Adsorption Isotherm

In general, inhibition by corrosion inhibitors for metal is affected by the concentration of absorbed molecules on metal substrate. Adsorption isotherm is a powerful tool to determine the adsorption mechanism of organic inhibitors on electrode surface. The data from potentiodynamic polarization curve tests were used to fit the adsorption isotherm. Among numerous of adsorption isotherms, such as El-Awady, Freundlich, Langmuir, Temkin, etc. As observed in Fig. 6, the best fitting is obtained at Langmuir adsorption model, because the relevant regression coefficient (R^2) is the largest and close to 1. Langmuir isotherm is shown as formula (4) [29, 30]:

$$C/\theta = 1/K_{ads} + C \quad (4)$$

where K_{ads} is equilibrium constant of adsorption, abscissa is C and ordinate is C/θ, intercept is shown as $1/K_{ads}$. The expression of standard adsorption Gibbs free energy (ΔG^0_{ads}) is equation (5) [9]:

$$K_{ads} = 1/55.5 \exp(-\Delta G^0_{ads} / RT) \quad (5)$$

Where R is 8.314 J $mol^{-1}k^{-1}$ and T is 298 K in present study. As seen in Fig. 6, the calculated ΔG^0_{ads} values for CPBI at 298 K is −31.35 kJ mol^{-1}. We all know that ΔG^0_{ads} values less negative than −20 kJ mol^{-1} indicates the process involved is a weak, physical adsorption type [31]. On the other hand, a strong type of chemisorption can be inferred if the ΔG^0_{ads} values are more negative than −40 kJ mol^{-1}. We can clearly see the standard adsorption Gibbs free energy is between −20 and −40 kJ mol^{-1} in Fig. 6. Therefore, the mixed adsorption type can be explained for the adsorption process of CPBI molecules on copper surface

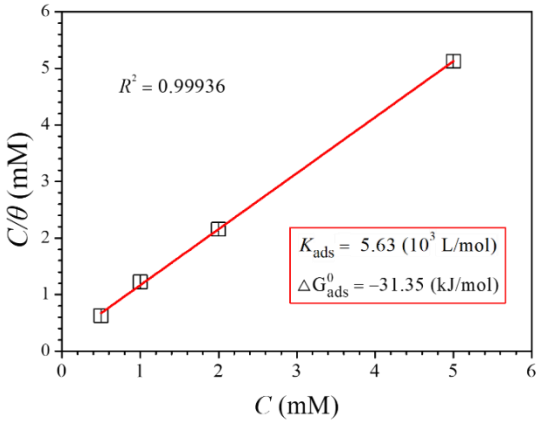

Figure 6. The Langmuir isotherm of copper with addition of CPBI in sulfuric acid at 298 K.

3.4 Morphology study

Fig. 7 shows the SEM images of copper surface immersed in 0.5 M H_2SO_4 in the absence and presence of CPBI for 48 h. From Fig. 7a, as seen that copper was uneven and there were many corrosion pits without the protection of inhibitor. After the addition of CPBI, the number of corrosion pits on the copper surface was significantly reduced and the surface became smooth. Besides, 3D LSCM images of copper sample soaked in 0.5 mol L^{-1} H_2SO_4 for 12 h with and without 5 mmol L^{-1} CPBI are shown in Fig. 8. It is clear that the entire copper surface becomes smooth and bright, and Ra values reduced from 0.453 μm to 0.113 μm after the addition of CPBI, indicating that CPBI effectively inhibit Cu corrosion in 0.5 mol L^{-1} H_2SO_4 solution. These observation shows the great protection ability of CPBI, which is may be owing to the adsorption of CPBI molecules on copper surface.

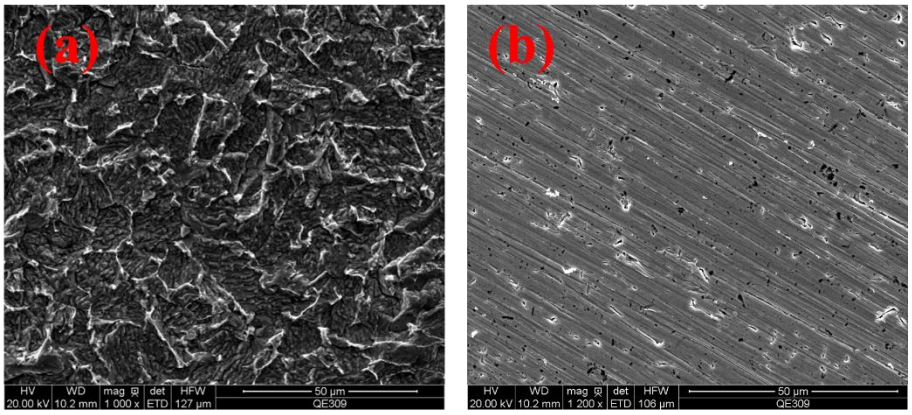

Figure 7. Copper samples immersed in (a) 0.5 mol L^{-1} H_2SO_4 and (b) 0.5 mol L^{-1} H_2SO_4 with 5 mmol L^{-1} CPBI for 48 h.

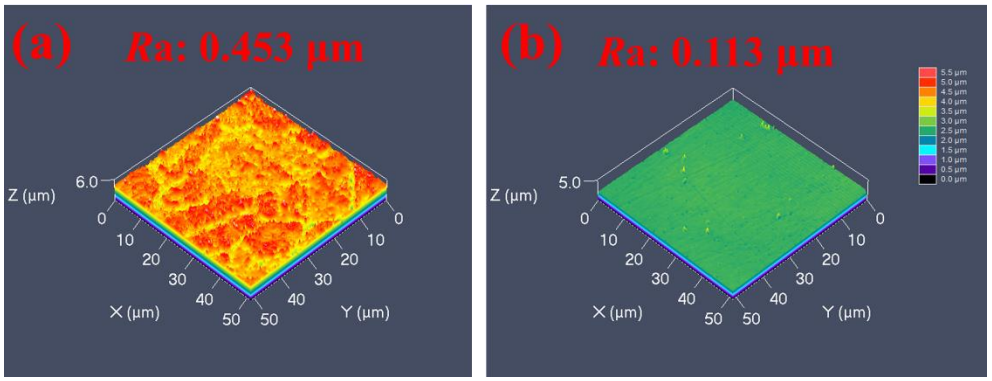

Figure 8. LSCM images (a) Copper sample soaked in 0.5 mol L^{-1} H_2SO_4 for 12 h, (c) copper sample soaked in 0.5 mol L^{-1} H_2SO_4 with 5 mmol L^{-1} CPBI for 12 h.

3.5 Quantum Chemical Calculation

DFT calculation was also used to reveal the adsorption and inhibition mechanism of CPBI on copper. Actually, CPBI molecule was optimized with DMol3 module to further study the relationship between the inhibition performance and the nature of CPBI molecule. The frontier molecular orbitals (FMO) are shown in Fig. 9 and corresponding quantum chemical parameters are listed in Table 3.

From Fig. 9, we can clearly see that HOMO and LOMO are both distributed throughout on whole CPBI molecule, indicating a parallel adsorption mode, which would accelerate form coordinate bonds with Cu substrate [32, 33]. Based on FMO theory, lower E_{LUMO} energy is related to a stronger electron-accepting ability, and higher energy of E_{HOMO} is often linked with a stronger electron-donating ability [34]. Therefore, it is generally believed that the smaller energy gap value, the more likely the molecules may have stronger interaction with metal and thus have good corrosion inhibition properties [35]. In this work, the low ΔE value of 3.10 eV for CPBI shown in Table 3 shows great inhibitive performance for copper corrosion. For the dipole moment, some researchers believe that the smaller the dipole moment, the more the accumulation of inhibitor molecules on metal to form a dense inhibitive layer, thus giving high corrosion inhibition capability. The μ value of CPBI molecule is 3.38 D, which is smaller compared

to other reports in the same system [2, 16, 36], which is a strong evidence that CPBI can have great inhibitive ability for copper corrosion.

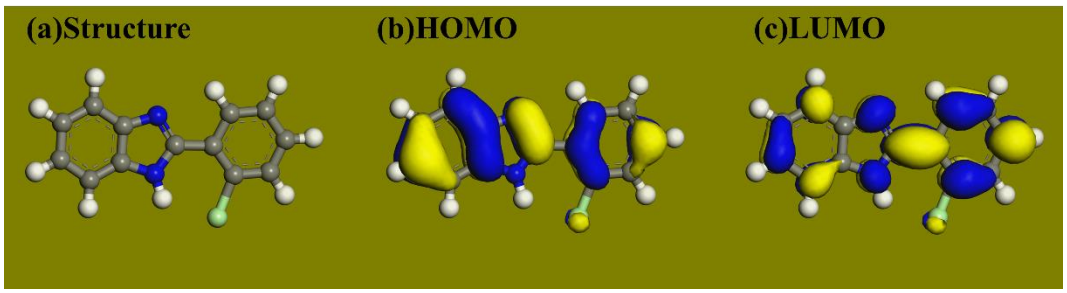

Figure 9. The molecular structure and frontier orbital diagrams of CPBI.

Table 3. The quantum chemical parameters of CPBI.

E_{HOMO}(eV)	E_{LUMO}(eV)	ΔE(eV)	μ(D)
–5.43	–2.33	3.10	3.38

3.6 MD

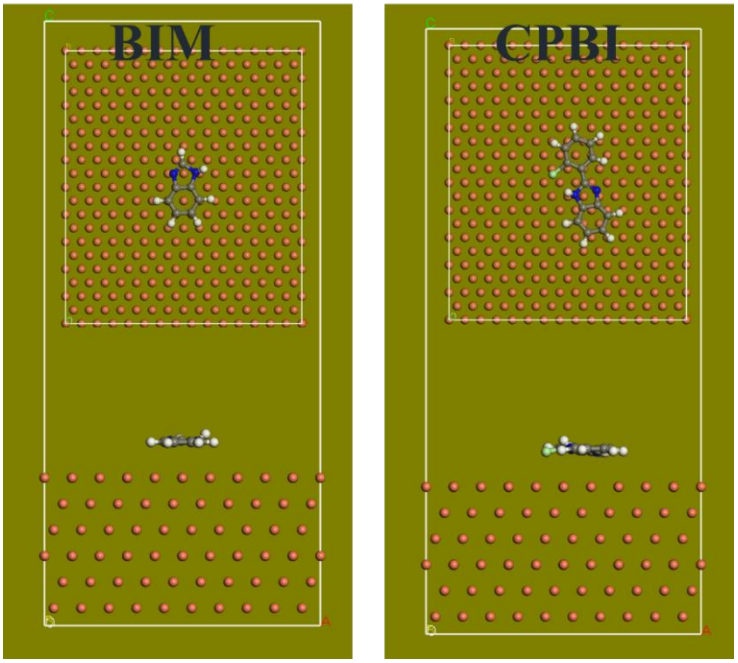

Figure 10. The stable adsorbed configuration of BIM and CPBI molecules on Cu (111), respectively.

The MD simulation has been considered as a promising simulation tool and was performed to study the adsorption behavior of CPBI and BIM molecules on Cu(111) surface to explain the inhibition improvement of CPBI. The stable adsorption configurations of these two molecules adsorbed on Cu (111) are shown in Fig. 10. Clearly, two molecules are both adsorbed on the copper surface in parallel.

Particularly, this mode can minimize the attack of corrosion particles to metal. Besides, the binding energy ($E_{binding}$) between copper and inhibitor molecules were also calculated by equation in the literature [19]. The obtained values of $E_{binding}$ is 34.3 kcal/mol for BIM and 65.2 kcal/mol for CPBI. Therefore, it can be drawn that CPBI inhibitor can exhibit superior inhibition performance than BIM because that CPBI can adsorb onto the steel surface easily and strongly [37-40]. The theoretical results can confirm its better experimental inhibition performance of CPBI than BIM above.

4. CONCLUSIONS

In this study, we have investigated CPBI as efficient inhibitors of copper corrosion in 1 mol L^{-1} H_2SO_4 solution. The inhibition performance increases with the increase of CPBI concentration because the adsorption of CPBI on copper surface. With the addition of 5 mmol L^{-1} CPBI, the maximum efficiencies of 92.3% was obtained, whereas 5 mmol L^{-1} BIM only have 70.1% ability. We also found that the adsorption of CPBI molecules on copper surface conforms to Langmuir type adsorption isotherm and belongs to a mixed type inhibitor. The surface morphology of SEM and LSCM and electrochemical tests are highly consistent. The ΔG_{ads}^{0} values indicate that CPBI adsorption on copper is chemisorbed and physical action to form compact layer, so it can give high inhibition performance. Finally, theoretical results showed that CPBI molecule has small dipole moment and energy gap and high $E_{binding}$ values, thus agree with those obtained experimentally.

References

1. Y. Qiang, S. Zhang, L. Guo, X. Zheng, B. Xiang, S. Chen, *Corros. Sci.*, 119 (2017) 68.
2. Y. Qiang, S. Zhang, S. Xu, L. Guo, N. Chen, I.B. Obot, *Inter. J. Electrochem. Sci.*, 11 (2016) 3147.
3. M.B.P. Mihajlovic, M.B. Radovanovic, Z.Z. Tasic, M.M. Antonijevic, *J. Mol. Liq.* 225 (2017) 127.
4. B. Tan, S. Zhang, H. Liu, Y. Qiang, W. Li, L. Guo, S. Chen, *J. Taiwan Instit. Chem. Eng.*, 102 (2019) 424.
5. M.n. Corrales-Luna, *Inter. J. Electrochem. Sci.*, (2019) 4420.
6. J. Du, *Inter. J. Electrochem. Sci.*, (2019) 4532.
7. Y. Qiang, S. Zhang, L. Wang, *Appl. Surf. Sci.*, 492 (2019) 228.
8. D.-Q. Zhang, L.-X. Gao, G.-D. Zhou, *Appl. Surf. Sci.*, 252 (2006) 4975.
9. Y. Qiang, S. Zhang, B. Tan, S. Chen, *Corros. Sci.*, 133 (2018) 6.
10. Y. Qiang, S. Zhang, Q. Xiang, B. Tan, W. Li, S. Chen, L. Guo, *RSC Adv.*, 8 (2018) 38860.
11. B. Tan, S. Zhang, H. Liu, Y. Guo, Y. Qiang, W. Li, L. Guo, C. Xu, S. Chen, *J. Colloid Interf. Sci.*, 538 (2019) 519.
12. H. M. Elabbasy, *Inter. J. Electrochem. Sci., (*2019) 3684.
13. A. S. Fouda, *Inter. J. Electrochem. Sci.*, (2019) 2187.
14. E.-S.M. Sherif, R.M. Erasmus, J.D. Comins, *Corros. Sci.*, 50 (2008) 3439.
15. M.A. Amin, K.F. Khaled, *Corros. Sci.*, 52 (2010) 1194.
16. Y.J. Qiang, S.T. Zhang, S.Y. Xu, L.L. Yin, *RSC Adv.*, 5 (2015) 63866.
17. R. Sabzi, R. Arefinia, *Corros. Sci.*, 153 (2019) 292.
18. R. Sadeghi Erami, M. Amirnasr, S. Meghdadi, M. Talebian, H. Farrokhpour, K. Raeissi, *Corros. Sci.*, 151 (2019) 190.
19. Y. Qiang, S. Zhang, S. Yan, X. Zou, S. Chen, *Corros. Sci.*, 126 (2017) 295.

20. Y. Qiang, S. Zhang, H. Zhao, B. Tan, L. Wang, *Corros. Sci.*, 161 (2019).
21. B. Tan, S. Zhang, Y. Qiang, L. Feng, C. Liao, Y. Xu, S. Chen, *J. Mol. Liq.* 248 (2017) 902.
22. J. Zhang, L. Zhang, G. Tao, *J. Mol. Liq.* 272 (2018) 369.
23. Y. Qiang, S. Zhang, L. Guo, S. Xu, L. Feng, I.B. Obot, S. Chen, *J. Clean Prod.*, 152 (2017) 17.
24. B. Tan, S. Zhang, W. Li, X. Zuo, Y. Qiang, L. Xu, J. Hao, S. Chen, *J. Ind. Eng. Chem.*, 77 (2019) 449.
25. C. Wang, *Inter. J. Electrochem. Sci., (*2019) 3443.
26. X. Wang, *Inter. J. Electrochem. Sci.*, (2019) 1178.
27. M. Murmu, K. Saha, N. Murmu, P. Banerjee, *Corros. Sci.*, 146 (2019) 134.
28. I.B. Onyeachu, I.B. Obot, A.A. Sorour, M.I. Abdul-Rashid, *Corros. Sci.*, 150 (2019) 183.
29. M.P. Casaletto, V. Figà, A. Privitera, M. Bruno, A. Napolitano, S. Piacente, *Corros. Sci.*, 136 (2018) 91.
30. A. Fitoz, H. Nazır, M. Özgür, E. Emregül, K.C. Emregül, *Corros. Sci.*, 133 (2018) 451.
31. J. Wang, Y. Qiang, L. Jiang, B. Xiang, S. Chen, S. Xing, Y. Wang, Y. Wang, *J. Mol. Liq.* 271 (2018) 959.
32. N.A. Wazzan, *J. Ind. Eng. Chem.* 26 (2015) 291.
33. M. Yadav, R.R. Sinha, T.K. Sarkar, I. Bahadur, E.E. Ebenso, *J. Mol. Liq.* 212 (2015) 686.
34. Y. Qiang, S. Fu, S. Zhang, S. Chen, X. Zou, *Corros. Sci.*, 140 (2018) 111.
35. Y. Qiang, S. Zhang, S. Xu, W. Li, *J. Colloid Interf. Sci.*, 472 (2016) 52.
36. Y. Qiang, L. Guo, S. Zhang, W. Li, S. Yu, J. Tan, *Sci. Rep.* 6 (2016) 33305.
37. L. Guo, S. Zhu, S. Zhang, Q. He, W. Li, *Corros. Sci.*, 87 (2014) 366.
38. I.B. Obot, Z.M. Gasem, *Corros. Sci.*, 83 (2014) 359.
39. L. Luo, S. Zhang, Y. Qiang, N. Chen, *Inter. J. Electrochem. Sci.*, 11 (2016) 8177.
40. L. Feng, S. Zhang, Y. Qiang, S. Xu, B. Tan, S. Chen, *Mater. Chem. Phys.*, 215 (2018) 229.